

## 2.8 $\mu\text{m}$ 中红外同步泵浦锁模光纤激光器

樊浩泽<sup>1,2</sup>, 梁金辉<sup>1</sup>, 郑树锴<sup>1</sup>, 蒋瑜<sup>1</sup>, 陈汉波<sup>1</sup>, 沈鹏生<sup>1</sup>, 李殿甲<sup>1,2</sup>, 於林鹏<sup>1</sup>,  
罗兴<sup>1</sup>, 王金章<sup>1</sup>, 闫培光<sup>1</sup>, 杜晨林<sup>2</sup>, 郭春雨<sup>1\*</sup>, 吕启涛<sup>3</sup>, 阮双琛<sup>1,2\*\*</sup>

<sup>1</sup>深圳大学物理与光电工程学院深圳市激光工程重点实验室, 广东 深圳 518060;

<sup>2</sup>深圳技术大学先进光学精密制造技术广东普通高校重点实验室, 广东 深圳 518118;

<sup>3</sup>大族激光科技股份有限公司, 广东 深圳 518000

**摘要** 2.8  $\mu\text{m}$  波段中红外光纤激光器在激光医疗领域具有重要的应用, 受到广泛关注。研究并实现了 2.8  $\mu\text{m}$  同步泵浦锁模脉冲光纤激光器。自主研制了大功率单模 976 nm 皮秒脉冲激光器并以此作为泵浦源, 以掺铒氟化物光纤环形腔作为谐振器, 通过纤芯同步泵浦的方式, 在交叉相位调制作用下实现了 2.8  $\mu\text{m}$  同步泵浦锁模脉冲激光器的制备。锁模脉冲的中心波长为 2784.7 nm, 重复频率为 6.534 MHz, 脉冲宽度接近光电探测器极限。所提方案不需要在谐振器内插入任何中红外主动或被动调制器, 具有系统稳定性好和易于实现全光纤化等优势。

**关键词** 激光器; 中红外激光; 同步泵浦锁模; 交叉相位调制

中图分类号 TN248 文献标志码 A

doi: 10.3788/CJL202249.0101020

### 1 引言

中红外激光(2~20  $\mu\text{m}$ )位于很多气体和有机分子的振转能级吸收带, 即所谓的“分子指纹区”<sup>[1]</sup>, 因此在疾病诊断<sup>[2-3]</sup>、远程遥感<sup>[4]</sup>、分子光谱学<sup>[5]</sup>以及军事国防<sup>[6]</sup>等领域具有重要的应用。其中, 2.8  $\mu\text{m}$  波段激光位于水吸收峰处, 在人体组织中的穿透深度浅、对周围邻近组织的损伤小, 可实现高效、安全的组织消融或切割, 因此具有高峰值功率的 2.8  $\mu\text{m}$  脉冲激光在医疗手术领域具有独特的应用价值<sup>[7]</sup>。

在众多中红外激光器实现方案中, 光纤激光器具有结构简单紧凑、散热性能好、输出功率高、光束质量好、可实现单横模运转等优势, 受到了广泛关注。中红外 2.8  $\mu\text{m}$  激光通常采用商用 976 nm 多模半导体激光器泵浦  $\text{Er}^{3+}:\text{ZBLAN}$  有源光纤来产生, 而具有高峰值功率的脉冲激光主要通过主动或被动调制器的锁模方式来获得。2015 年, Tang 等<sup>[8]</sup>基于半导体可饱和吸收镜(SESAM)实现了平

均功率为 1.05 W、脉宽为 25 ps 的 2.8  $\mu\text{m}$  锁模脉冲输出。随后, 研究者们基于石墨烯<sup>[9]</sup>、黑磷<sup>[10]</sup>以及过渡金属硫化物<sup>[11]</sup>等新型二维材料可饱和吸收体, 也实现了 2.8  $\mu\text{m}$  中红外光纤被动锁模脉冲激光的制备。然而, 这些可饱和吸收体二维材料都面临着易损伤及潮解和氧化导致的长期使用性能下降等问题<sup>[12]</sup>。此外, 基于非线性偏振旋转演化(NPE)效应的“人工可饱和吸收体”也被用于实现 2.8  $\mu\text{m}$  波段锁模脉冲激光器的制备<sup>[13-18]</sup>。NPE 环形腔锁模具有 100% 的理论最大调制深度和理想的飞秒超快恢复时间, 可以实现飞秒孤子态的锁模脉冲。2020 年, Gu 等<sup>[18]</sup>基于 NPE 锁模技术, 获得了脉宽为 131 fs、平均输出功率为 317 mW、重复频率为 107 MHz 的 2.8  $\mu\text{m}$  锁模脉冲输出。对于 NPE 被动锁模光纤激光器, 外界温度和应变等环境因素对锁模启动和运转有严重的影响, 环境的变化容易引起偏振态的改变, 进而导致系统失锁。2019 年, Majewski 等<sup>[19]</sup>基于频移反馈技术(FSF), 利用声光调制器实现了脉宽为 5 ps 的 2.86  $\mu\text{m}$  锁模脉冲, 并

收稿日期: 2021-09-13; 修回日期: 2021-10-14; 录用日期: 2021-10-25

基金项目: 国家自然科学基金(61975136, 61935014, 61775146)、广东省自然科学基金(2019A1515010699)、深圳市承接国家重大科技项目(CJGJZD20200617103003009)

通信作者: \*cyguo@szu.edu.cn; \*\*scruan@sztu.edu.cn

在此基础上进一步实现了波长可调谐<sup>[20]</sup>。然而,中红外主动调制器的价格高昂,且为自由空间结构,在谐振腔中引入主动调制器会提高系统的复杂性和成本,而且无法实现全光纤结构。

综上所述,目前中红外光纤激光器锁模脉冲的产生不仅受限于主动和被动调制器件,还面临着与锁模技术相关联的系统稳定性问题。因此,克服相关的限制以实现长期稳定可靠的中红外锁模脉冲输出将会对中红外脉冲激光的研究和应用具有重要的价值,而同步泵浦锁模技术提供了一个解决思路。同步泵浦锁模技术是指通过采用重复频率等于谐振腔基频整数倍的脉冲激光同步泵浦,进而对信号光进行调制以实现锁模脉冲输出的方法<sup>[21-22]</sup>。该技术最早应用于色心<sup>[23]</sup>、钛宝石<sup>[24]</sup>、拉曼激光器<sup>[25]</sup>以及染料激光器<sup>[26]</sup>中,是产生脉冲激光的重要技术。传统同步泵浦锁模是通过脉冲泵浦光对激光进行同步增益调制,要求增益介质上能级具有较短的寿命,以利于快速弛豫过程<sup>[27]</sup>,而光纤激光器的上能级寿命较长,难以提供足够快速的增益调制。

事实上,脉冲泵浦光除了在激光器中引入增益调制外,还引入了交叉相位调制。如果能提供具有高峰值功率的 976 nm 单横模脉冲激光作为泵浦源,在泵浦光的重复频率为谐振腔基频整数倍的同步泵浦条件下,利用泵浦光和信号激光在光纤谐振腔中的交叉相位调制作用,也有望实现 2.8  $\mu\text{m}$  同步泵浦锁模脉冲的产生。在交叉相位调制过程中,利用泵浦脉冲在光纤中产生强烈的非线性作用对信号激光相位进行周期性调制,其非线性相移可以表示为

$$\Delta\varphi_{\max} = 2n_2 k_s PL / A_{\text{core}}, \quad (1)$$

式中: $P$  为峰值功率; $n_2 = 3.2 \times 10^{-20} \text{ m}^2/\text{W}$  为非线性折射率; $k_s$  为信号波长的真空波数; $L$  为交叉相位调制作用距离; $A_{\text{core}}$  为纤芯面积。可以看出,更高的泵浦光峰值功率、更长的作用距离和更小的模场面积可以使交叉相位调制作用更强。1993 年,Stock 等<sup>[28]</sup>报道了基于同步泵浦锁模技术的光纤激光器,利用重复频率为 100 MHz、脉宽为 70 ps、平均功率为 300 mW 的 Nd:YAG 激光器,同步泵浦线形腔  $\text{Er}^{3+}/\text{Yb}^{3+}$  共掺光纤激光器,获得了脉宽为 2.4 ps 的 1.5  $\mu\text{m}$  锁模脉冲。2019 年,本课题组采用脉冲重复频率为 12.38 MHz、脉宽为 23.59 ps 的 1550 nm 光纤激光器作为泵浦源,对 2  $\mu\text{m}$  掺铋环形腔进行同步泵浦,获得了脉宽为 880 fs 的锁模脉冲<sup>[29]</sup>。同步泵浦锁模光纤激光器需要单模高光束

质量的脉冲激光作为泵浦源,而常规用于掺铋氟化物光纤激光器的半导体激光泵浦源难以满足这一要求,从而限制了同步泵浦锁模技术在中红外光纤激光器中的应用,关于中红外同步泵浦锁模光纤激光器的研究鲜有报道。

本文通过同步泵浦技术,在交叉相位调制作用下,实现了 2.8  $\mu\text{m}$  中红外同步泵浦锁模光纤激光器。这一方案不需要在谐振腔内插入任何主动和被动调制器件,因此基于同步泵浦锁模技术的光纤激光器具有较高的系统稳定性,而且有望实现全光纤化的中红外锁模脉冲光纤激光器。

## 2 实验装置

本文采用 976 nm 大功率单模脉冲光纤激光器作为 2.8  $\mu\text{m}$  激光泵浦源,该泵浦源包括重复频率和脉宽可调的 976 nm 增益开关半导体激光器种子源和两级单模主振荡功率放大(MOPA)系统。泵浦激光器的实验结构如图 1 所示:有源光纤使用的是 YDF-PM-DC-13/80 保偏双包层环掺杂  $\text{Yb}^{3+}$  光纤,纤芯直径为 13  $\mu\text{m}$ ,包层直径为 80  $\mu\text{m}$ ,内包层数值孔径  $NA = 0.45$ ,掺杂浓度(摩尔分数)为 0.16%。采用掺锗无源双包层光纤(GDF)与有源光纤进行模场匹配,其纤芯直径为 10  $\mu\text{m}$ ,内包层直径为 80  $\mu\text{m}$ 。另外,在实验结构中,环形器结合光纤布拉格光栅(FBG)用以滤除 976 nm 附近的放大自发辐射光(ASE),FBG 的中心波长( $\lambda_c$ )为 976.5 nm,3 dB 带宽( $\Delta\lambda$ )为 0.85 nm。976 nm 带通滤波器(BPF)滤除 1  $\mu\text{m}$  波段的 ASE,光耦合器(OC)用来监控一级放大激光信号。合束器泵浦单端的最大承受功率为 80 W,采用包层泵浦光剥离器(CPS)滤除包层中剩余的泵浦光。二级放大器尾纤为 PM1060L 单模光纤,采用 8°角切割,避免了激光放大过程中在光纤端面形成的反射损坏器件,976 nm 隔离器(ISO)防止激光返回上一级。二级放大器还采用半导体制冷器(TEC)在有源光纤熔接点处制冷以保证激光器长时间高功率工作。

2.8  $\mu\text{m}$  同步泵浦锁模光纤激光器的实验结构如图 2 所示。以上述的 976 nm 大功率单模脉冲光纤激光器作为泵浦源。利用焦距为 15 mm 的平凸石英透镜 L1 对 976 nm 泵浦光进行准直处理,再利用一个焦距为 20 mm 的  $\text{CaF}_2$  平凸透镜 L2 进行聚焦并将激光耦合进入氟化物光纤。在两个透镜间放置一个 976 nm 高透(HT)、2.8  $\mu\text{m}$  高反(HR)的 45°二色镜 DM1。实验结构中的光纤部分包括有源

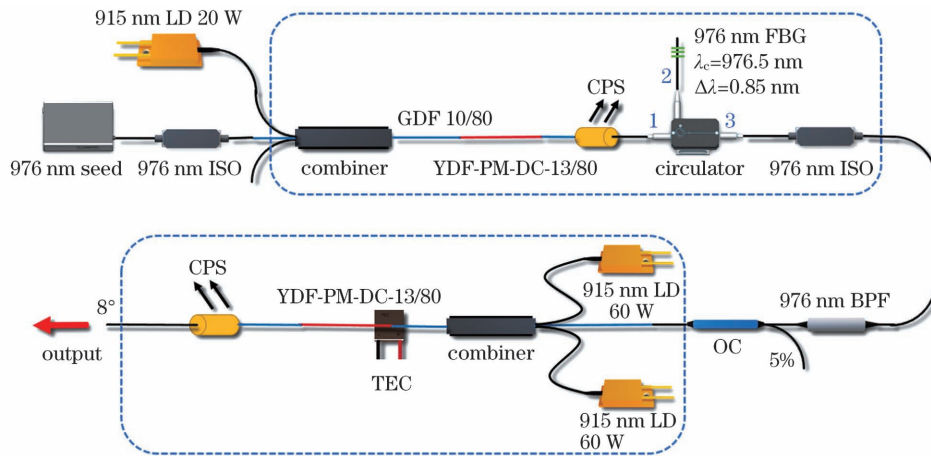
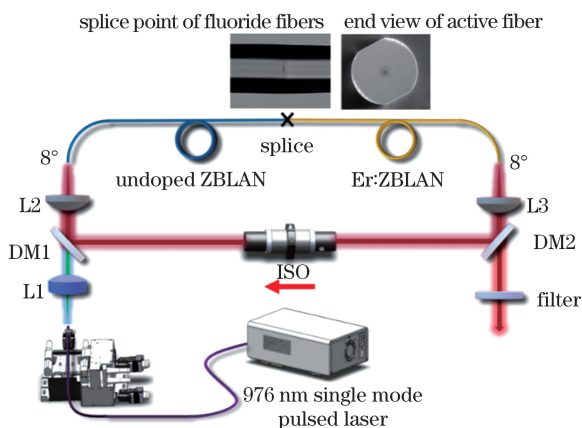


图 1 976 nm 泵浦激光器的实验装置示意图

Fig. 1 Schematic of experimental setup of 976 nm pump laser

光纤和无源光纤,两种光纤通过 Vytran GPX 3400 大芯径光纤熔接机进行熔接,熔接效果如图 2 左插图所示。光纤的前段是长度为 22 m 的单包层无源 ZBLAN 光纤,纤芯直径为 14  $\mu\text{m}$ , NA 为 0.125,包层直径为 250  $\mu\text{m}$ ,经过实验测试,无源光纤对 976 nm 激光的损耗小于 0.01 dB/m;后段是长度为 8.5 m 的掺  $\text{Er}^{3+}$ :ZBLAN 双包层有源光纤,纤芯直径为 16.5  $\mu\text{m}$ , NA 为 0.125,内包层(双 D 型)尺寸为  $240 \times 260 \mu\text{m}$ ,如图 2 右插图所示,外包层直径为 290  $\mu\text{m}$ , NA 为 0.4,掺杂浓度(摩尔分数)为 1%。在腔前端引入无源光纤一方面是为了增加 2.8  $\mu\text{m}$  信号光和泵浦光的交叉相位调制作用距离,避免有源光纤中  $\text{Er}^{3+}$  离子对 976 nm 泵浦光的过早吸收,另外一方面是降低激光脉冲重复频率,提高泵浦光峰值功率。

图 2 2.8  $\mu\text{m}$  激光器的实验装置示意图Fig. 2 Schematic of experimental setup of 2.8  $\mu\text{m}$  laser

无源光纤前端和有源光纤后端切割  $8^\circ$  角以抑制 2.8  $\mu\text{m}$  寄生激光。有源光纤输出端通过焦距为 20 mm 的  $\text{CaF}_2$  透镜 L3 后被准直,并使用  $45^\circ$  二色

镜 DM2(HT@976 nm, 反射率  $R=70\%$ @2.8  $\mu\text{m}$ ) 将 70% 的 2.8  $\mu\text{m}$  激光功率反射回腔内,30% 的 2.8  $\mu\text{m}$  激光输出,输出光中的剩余泵浦光被一个滤波片滤除。返回腔内的 2.8  $\mu\text{m}$  激光通过一个偏振相关隔离器后呈单向运转,环形腔总腔长为 31 m,对应的脉冲重复频率为 6.534 MHz。

采用带宽为 200 MHz 的红外 HgCdTe 探测器,20 GHz 示波器以及射频频谱分析仪对锁模脉冲的时域和频域参数进行测量,利用光谱仪(分辨率为 0.1 nm)对锁模脉冲进行光谱测量。

### 3 实验结果与分析

调节 976 nm 脉冲光纤激光器的重复频率至 6.534 MHz,以匹配 2.8  $\mu\text{m}$  激光环形腔(总腔长 31 m)。对于 976 nm 泵浦激光器,976 nm 种子光输出功率为 80  $\mu\text{W}$ ,一级放大系统将其放大至 20 mW,二级放大系统的激光功率输出特性如图 3 所示。图 3(a)为 976 nm 激光输出功率随 915 nm 泵浦光功率的变化情况,斜率效率为 5.3%,当二级泵浦功率为 75 W 时,输出功率为 3.7 W,此时未达到功率饱和,且有源光纤处的熔接点温度仅为  $30^\circ\text{C}$ 。图 3(b)为输出功率为 2.5 W 时测试的功率稳定性,3 h 内的最大功率波动幅度小于 2%。

当泵浦脉冲的平均功率为 1.55 W 时,2.8  $\mu\text{m}$  激光的输出功率为 2.5 mW,此时通过调节泵浦脉冲的重复频率,可以观察到 2.8  $\mu\text{m}$  锁模脉冲输出。在继续增加泵浦功率至 2.5 W 的过程中,信号光的光谱和时域包络变化不明显,2.8  $\mu\text{m}$  激光的最大输出功率为 15 mW。本文采用了低掺杂  $\text{Er}^{3+}$  有源光纤(摩尔分数为 1%),难以突破  $\text{Er}^{3+}$  离子 2.8  $\mu\text{m}$  发射激光下能级寿命长于上能级寿命导致的粒子数

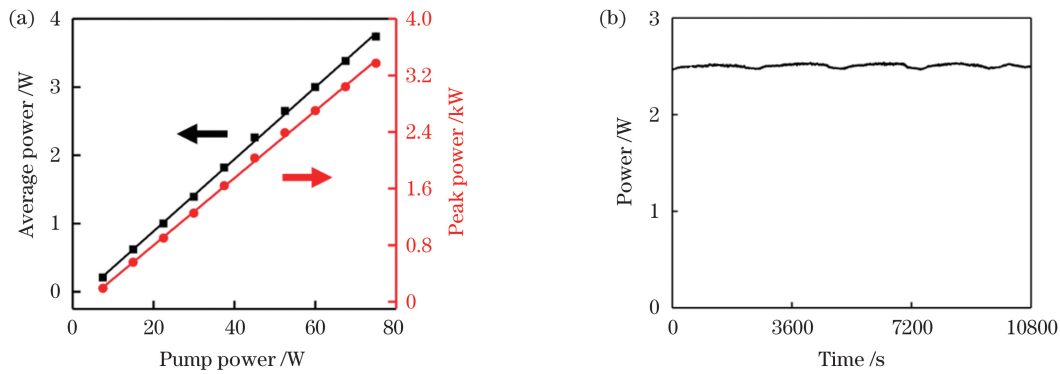


图 3 976 nm 激光器功率输出特性。(a)输出功率随泵浦功率的变化;(b)输出功率的稳定性测试

Fig. 3 Power output characteristics of 976 nm laser. (a) Output power versus pump power; (b) stability test of output power

瓶颈,因此  $2.8 \mu\text{m}$  输出激光的斜率效率相对较低。当采用高掺杂有源光纤时,其高吸收系数会在纤芯泵浦方案中导致熔接点处形成强烈的端面热效应,系统难以长时间稳定工作。

当泵浦功率为  $1.6 \text{ W}$  时,对应的泵浦脉冲激光的输出特性如图 4 所示。图 4(a)为泵浦脉冲波形,其半峰全宽(FWHM)为  $170 \text{ ps}$ 。图 4(b)为输出脉

冲序列,其周期为  $153 \text{ ns}$ 。图 4(c)是基频处的射频谱,基频信噪比为  $67 \text{ dB}$ ,插图为  $0 \sim 2 \text{ GHz}$  范围内的射频谱。图 4(d)为泵浦脉冲的输出光谱,虚线为种子光光谱,实线为主振荡功率放大系统最终的输出光谱。由于  $976 \text{ nm}$  激光功率较小( $80 \mu\text{W}$ ),重复频率较低且脉宽较窄, $976 \text{ nm}$  附近的泵浦信号光 ASE 信噪比为  $14 \text{ dB}$ 。

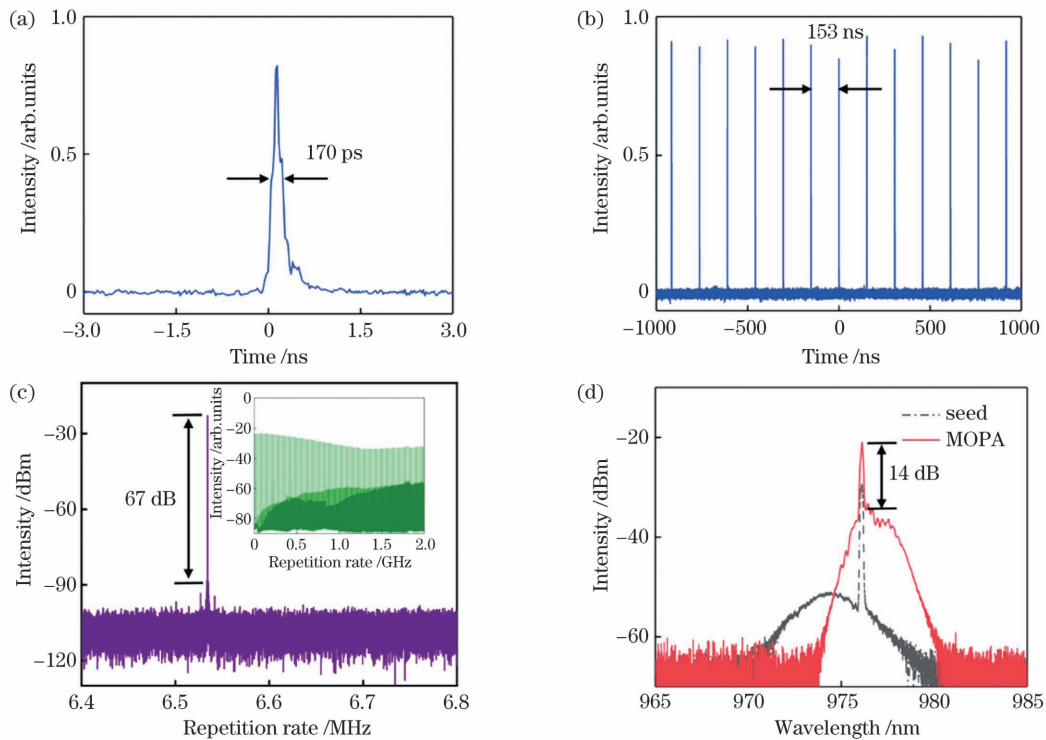


图 4 976 nm 单模泵浦激光器的脉冲特性。(a)单脉冲波形;(b)脉冲序列;(c)射频谱;(d)输出光谱

Fig. 4 Pulse characteristics of 976 nm single-mode pump laser. (a) Waveform of single pulse; (b) pulse train; (c) radio frequency spectrum; (d) output spectra

当  $2.8 \mu\text{m}$  激光的输出功率为  $3 \text{ mW}$  时,实验结果如图 5 所示。单脉冲形状如图 5(a)所示,其 FWHM 为  $3.1 \text{ ns}$ (接近带宽为  $200 \text{ MHz}$  的探测器可测量的极限脉宽),由于输出功率较低,未能利用

自相关仪测出脉宽。图 5(b)为脉冲序列,周期为  $153 \text{ ns}$ ,与泵浦光脉冲周期相对应。图 5(c)是采用频谱仪测试的基频与  $300 \text{ MHz}$  内的射频谱(插图),基频信噪比为  $48 \text{ dB}$ ,基频两侧的边带表示脉冲波

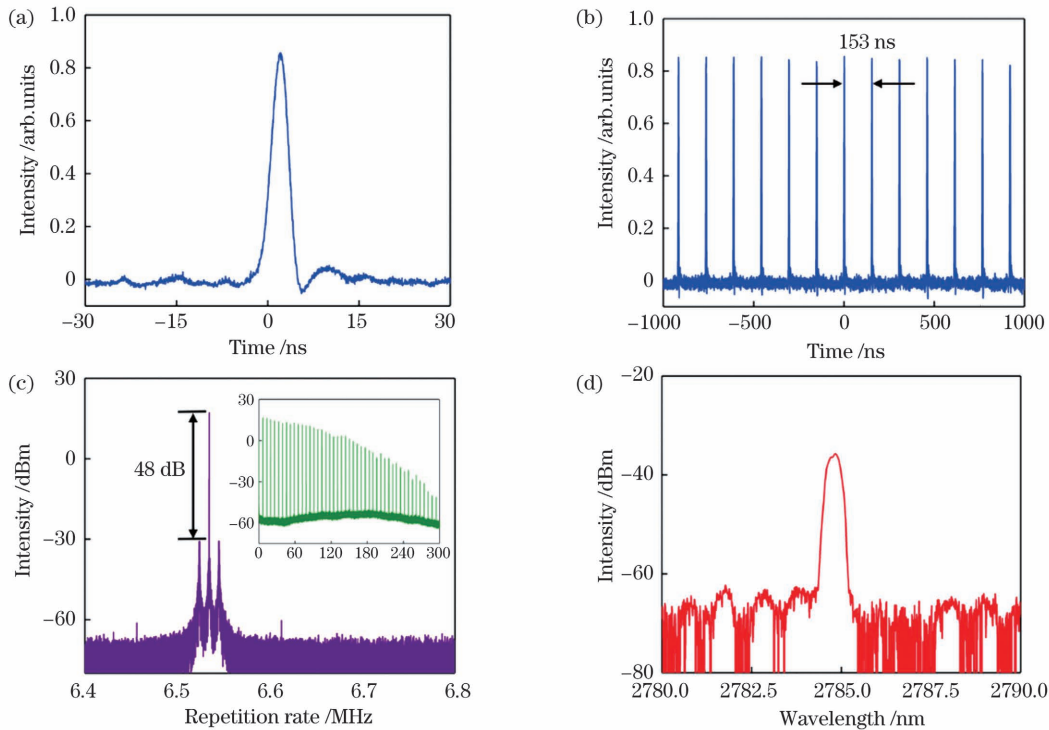


图 5 2.8  $\mu\text{m}$  同步泵浦锁模激光器的脉冲输出特性。(a) 单脉冲波形; (b) 脉冲序列; (c) 射频谱; (d) 输出光谱

Fig. 5 Pulse output characteristics of 2.8  $\mu\text{m}$  synchronously pumped mode-locked laser. (a) Waveform of single pulse;

(b) pulse train; (c) radio frequency spectrum; (d) output spectrum

形在时域上的大范围幅度抖动,这是调 Q 锁模或锁模激光器中常见的弛豫振荡现象<sup>[8, 30]</sup>,在同步泵浦锁模过程中,即使腔长与泵浦光频率严格匹配,由于偏振态、损耗扰动等原因,输出脉冲幅度也会不断抖动,且弛豫振荡频率与激光腔长呈反比<sup>[31-32]</sup>。图 5(d)为 2.8  $\mu\text{m}$  激光输出光谱,中心波长为 2784.7 nm, 3 dB 谱宽为 0.4 nm。实验中发现,调节脉冲重复频率,使其偏离中心频率 200 Hz 时,脉冲消失,即最大重复频率失谐量为  $\pm 200$  Hz,对应大约  $\pm 1$  mm 的腔长失谐。重复频率的窄范围可调而不失锁一般是激光波长自适应变化或偏振态变化导致的折射率变化引起的。最后,在 2 h 长时间测试过程中,没有出现失锁现象,锁模可实现自启动,在泵浦功率足够的情况下,当泵浦光重复频率与 2.8  $\mu\text{m}$  激光器基频匹配时,即可获得 2.8  $\mu\text{m}$  锁模脉冲输出。

实验中还考虑了泵浦光和信号光的群速度失配问题。对于同步泵浦来说,泵浦脉冲的群速度应该尽量与腔内循环的 2.8  $\mu\text{m}$  信号光匹配。对于成分为 55.8ZrF<sub>4</sub>-14.4BaF<sub>2</sub>-5.8LaF<sub>3</sub>-3.8AlF<sub>3</sub>-20.2NaF 的 ZBLAN 光纤,不同波长处的纤芯折射率由 Sellmeier 方程<sup>[33]</sup>决定:

$$cn^2(\lambda) - 1 = \frac{1.168\lambda^2}{\lambda^2 - 0.0954^2} + \frac{2.77\lambda^2}{\lambda^2 - 25^2}, \quad (2)$$

式中:  $\lambda$  为入射波长;  $c = 3 \times 10^8$  m/s 为光速;  $n(\lambda)$  为纤芯折射率。对于泵浦波长 976 nm 和信号光波长 2784 nm, 群折射率分别为  $N_g^{976} = 1.485383$  和  $N_g^{2784} = 1.486064$ , 群速度失配量为 2.27 ps/m, 因此,当 976 nm 泵浦脉宽为 170 ps 时,在 30.5 m 光纤中传输可以保证泵浦光和信号光相互作用而不走离。

为了进一步验证锁模原理,我们开展了反向泵浦的实验,实验结构如图 6 所示,其与图 2 不同之处在于隔离器反向放置。这时 976 nm 泵浦光与 2.8  $\mu\text{m}$  信号光以相反方向传输,几乎不存在交叉相位调制作用,即使在泵浦功率为 2.7 W 时,依然没有获得 2.8  $\mu\text{m}$  锁模脉冲,正反向泵浦时的输出时域波形对比如图 7 所示,证实了本文同步泵浦锁模脉冲的产生并非基于增益调制作用。

对于正向泵浦,当在 2.8  $\mu\text{m}$  环形腔内仅使用 8.5 m 双包层有源光纤且其他结构相同时,未能获得 2.8  $\mu\text{m}$  锁模脉冲。因为如果只采用有源光纤,随着 976 nm 泵浦光不断被增益介质中的 Er<sup>3+</sup> 吸收,功率不断衰减,交叉相位调制作用减弱且作用距离减短;另外,由于腔长减小,脉冲重复频率增大,在相同泵浦平均功率下,泵浦光的峰值功率降低,不足以提供锁模所需的非线性相移。因此,实验中在泵

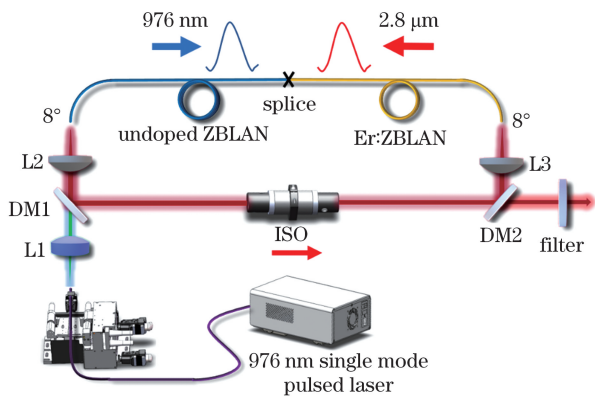
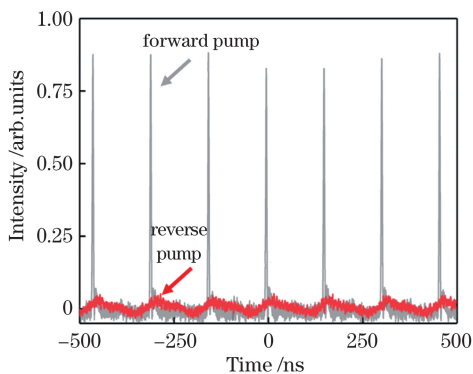
图 6 反向泵浦 2.8  $\mu\text{m}$  激光实验装置示意图Fig. 6 Schematic of experimental setup of reverse-pumped 2.8  $\mu\text{m}$  laser

图 7 反向泵浦与正向泵浦下的输出时域波形对比

Fig. 7 Comparison of output time domain waveforms under reverse pump and forward pump

浦光入射端加入一段较长的无源光纤,使得泵浦光在未经有源光纤的吸收时与信号光相互作用,产生较强的交叉相位调制作用,从而实现了锁模。这也进一步证明了交叉相位调制是实现锁模的主要原因。

## 4 结 论

提出并实现了 976 nm 单模脉冲激光器泵浦的 2.8  $\mu\text{m}$  同步泵浦锁模脉冲光纤激光器,其重复频率为 6.534 MHz,中心波长为 2784.7 nm,3 dB 谱宽为 0.4 nm,最大输出功率为 15 mW。由于输出功率较低,难以通过自相关仪探测其实际脉宽,但通过示波器显示为 3.1 ns,接近光电探测器的探测极限脉宽。由于其谱宽较窄,傅里叶变换极限脉宽也仅为 21 ps。接下来将会进一步优化并提升 976 nm 泵浦光质量、采用纤芯更细的氟化物光纤以增强交叉相位调制作用、选择掺杂浓度相对较高的有源光纤以提高输出功率,实现中红外超短锁模脉冲。总之,基于同步泵浦锁模技术,不需要在谐振腔中引入

任何主动或被动调制器件,而且系统结构简单,稳定性好,易于全光纤化。研究结果为在中红外波段实现稳定可靠锁模脉冲激光器提供了一种方案。

## 参 考 文 献

- [1] Hu M L, Cai Y. Research progress on mid-infrared ultrafast fiber laser [J]. Chinese Journal of Lasers, 2020, 47(5): 0500009.  
胡明列,蔡宇. 中红外波段超快光纤激光器研究进展 [J]. 中国激光, 2020, 47(5): 0500009.
- [2] Pratisto H, Frenz M, Ith M, et al. Temperature and pressure effects during erbium laser stapledotomy [J]. Lasers in Surgery and Medicine, 1996, 18(1): 100-108.
- [3] Skorczakowski M, Swiderski J, Pichola W, et al. Mid-infrared Q-switched Er:YAG laser for medical applications [J]. Laser Physics Letters, 2010, 7(7): 498-504.
- [4] Bae T W, Kim B I, Kim Y C, et al. Jamming effect analysis of infrared reticle seeker for directed infrared countermeasures [J]. Infrared Physics & Technology, 2012, 55(5): 431-441.
- [5] Paldus B A, Harb C C, Spence T G, et al. Cavity ringdown spectroscopy using mid-infrared quantum-cascade lasers [J]. Optics Letters, 2000, 25(9): 666-668.
- [6] Th Bekman H H P, van den Heuvel J C, van Putten F J M, et al. Development of a mid-infrared laser for study of infrared countermeasures techniques [J]. Proceedings of SPIE, 2004, 5615: 27-38.
- [7] Walsh B M. Review of Tm and Ho materials; spectroscopy and lasers [J]. Laser Physics, 2009, 19(4): 855-866.
- [8] Tang P, Qin Z, Liu J, et al. Watt-level passively mode-locked Er<sup>3+</sup>-doped ZBLAN fiber laser at 2.8  $\mu\text{m}$  [J]. Optics Letters, 2015, 40(21): 4855-4858.
- [9] Zhu G W, Zhu X S, Wang F Q, et al. Graphene mode-locked fiber laser at 2.8  $\mu\text{m}$  [J]. IEEE Photonics Technology Letters, 2016, 28(1): 7-10.
- [10] Qin Z, Xie G, Zhao C, et al. Mid-infrared mode-locked pulse generation with multilayer black phosphorus as saturable absorber [J]. Optics Letters, 2016, 41(1): 56-59.
- [11] Guo C Y, Wei J C, Yan P G, et al. Mode-locked fiber laser at 2.8  $\mu\text{m}$  using a chemical-vapor-deposited WSe<sub>2</sub> saturable absorber mirror [J]. Applied Physics Express, 2020, 13(1): 012013.
- [12] Dong Z K, Song Y R. Research progress of mode-locked fiber lasers based on saturable absorbers [J]. Chinese Journal of Lasers, 2021, 48(5): 0501006.

- 董自凯, 宋晏蓉. 光纤激光器被动锁模技术研究进展 [J]. 中国激光, 2021, 48(5): 0501006.
- [13] Duval S, Bernier M, Fortin V, et al. Femtosecond fiber lasers reach the mid-infrared [J]. *Optica*, 2015, 2(7): 623-626.
- [14] Hu T, Jackson S D, Hudson D D. Ultrafast pulses from a mid-infrared fiber laser [J]. *Optics Letters*, 2015, 40(18): 4226-4228.
- [15] Duval S, Gauthier J C, Robichaud L R, et al. Watt-level fiber-based femtosecond laser source tunable from 2.8  $\mu\text{m}$  to 3.6  $\mu\text{m}$  [J]. *Optics Letters*, 2016, 41(22): 5294-5297.
- [16] Gu H, Qin Z P, Xie G Q, et al. Generation of 131 fs mode-locked pulses from 2.8  $\mu\text{m}$  Er:ZBLAN fiber laser [J]. *Chinese Optics Letters*, 2020, 18(3): 031402.
- [17] Huang J, Pang M, Jiang X, et al. Sub-two-cycle octave-spanning mid-infrared fiber laser [J]. *Optica*, 2020, 7(6): 574-579.
- [18] Gu H A, Qin Z P, Xie G Q, et al. Generation of 131 fs mode-locked pulses from 2.8  $\mu\text{m}$  Er:ZBLAN fiber laser [J]. *Chinese Optics Letters*, 2020, 18(3): 031402.
- [19] Majewski M R, Woodward R I, Jackson S D. Ultrafast mid-infrared fiber laser mode-locked using frequency-shifted feedback [J]. *Optics Letters*, 2019, 44(7): 1698-1701.
- [20] Pawliszewska M, Majewski M R, Jackson S D. Electronically tunable picosecond pulse generation from Ho<sup>3+</sup>-doped fluoride fiber laser using frequency-shifted feedback [J]. *Optics Letters*, 2020, 45(20): 5808-5811.
- [21] Wang Y, Set S Y, Yamashita S. Active mode-locking via pump modulation in a Tm-doped fiber laser [J]. *APL Photonics*, 2016, 1(7): 071303.
- [22] Li G, Zhou Y, Li S J, et al. Synchronously pumped mode-locked 1.89  $\mu\text{m}$  Tm-doped fiber laser with high detuning toleration [J]. *Chinese Physics Letters*, 2018, 35(11): 114203.
- [23] Kelly S, New G H C, Wood D. Mode-locking dynamics of synchronously-pumped colour-centre lasers [J]. *Applied Physics B*, 1988, 47(4): 349-357.
- [24] Mollenauer L F, Vieira N D, Szeto L. Mode locking by synchronous pumping using a gain medium with microsecond decay times [J]. *Optics Letters*, 1982, 7(9): 414-416.
- [25] Chen H, Chen S P, Jiang Z F, et al. All-fiberized synchronously pumped 1120 nm picosecond Raman laser with flexible output dynamics [J]. *Optics Express*, 2015, 23(18): 24088.
- [26] Kuhl J, Klingenberg H, Linde D. Picosecond and subpicosecond pulse generation in synchronously pumped mode-locked cw dye lasers [J]. *Applied Physics*, 1979, 18(3): 279-284.
- [27] Okhotnikov O G, Guina M, Pessa M. Stabilization of passive harmonic mode-locking by amplitude modulation [J]. *IEEE Photonics Technology Letters*, 2002, 14(2): 146-148.
- [28] Stock M L, Yang L M, Andrejco M J, et al. Synchronous mode locking using pump-induced phase modulation [J]. *Optics Letters*, 1993, 18(18): 1529.
- [29] Huang S T, Zhang S L, Guo C Y, et al. 2  $\mu\text{m}$  thulium-doped fiber laser based on synchronously pumped mode-locking [C] // 2019 Photonics & Electromagnetics Research Symposium-Fall (PIERS-Fall), December 17-20, 2019, Xiamen, China. New York: IEEE Press, 2019: 1628-1631.
- [30] Haboucha A, Fortin V, Bernier M, et al. Fiber Bragg grating stabilization of a passively mode-locked 2.8  $\mu\text{m}$  Er<sup>+3</sup>: fluoride glass fiber laser [J]. *Optics Letters*, 2014, 39(11): 3294-3297.
- [31] Weingarten K J, Braun B, Keller U. *In situ* small-signal gain of solid-state lasers determined from relaxation oscillation frequency measurements [J]. *Optics Letters*, 1994, 19(15): 1140-1142.
- [32] Schlatter A, Zeller S C, Grange R, et al. Pulse-energy dynamics of passively mode-locked solid-state lasers above the Q-switching threshold [J]. *Journal of the Optical Society of America B*, 2004, 21(8): 1469-1478.
- [33] Wei Q, Yu B B, Huang T Y, et al. Mid-infrared high repetition mode-locked laser based on cross-band all-optical injection modulation [J]. *Laser Physics Letters*, 2020, 17(6): 065101.

## 2.8 $\mu\text{m}$ Mid-Infrared Synchronously Pumped Mode-Locked Fiber Laser

Fan Haoze<sup>1,2</sup>, Liang Jinhui<sup>1</sup>, Zheng Shukai<sup>1</sup>, Jiang Yu<sup>1</sup>, Chen Hanbo<sup>1</sup>, Shen Pengsheng<sup>1</sup>,  
Li Dianjia<sup>1,2</sup>, Yu Linpeng<sup>1</sup>, Luo Xing<sup>1</sup>, Wang Jinzhang<sup>1</sup>, Yan Peiguang<sup>1</sup>, Du Chenlin<sup>2</sup>,  
Guo Chunyu<sup>1</sup>, Lü Qitao<sup>3</sup>, Ruan Shuangchen<sup>1,2\*</sup>

<sup>1</sup> Shenzhen Key Laboratory of Laser Engineering, College of Physical and Optoelectronic Engineering,  
Shenzhen University, Shenzhen, Guangdong 518060, China;

<sup>2</sup> Key Laboratory of Advanced Optical Precision Manufacturing Technology of Guangdong Higher Education Institutes,  
Shenzhen Technology University, Shenzhen, Guangdong 518118, China;

<sup>3</sup> Han's Laser Technology Co., Ltd., Shenzhen, Guangdong 518000, China

### Abstract

**Objective** 2.8  $\mu\text{m}$  pulsed laser sources are ideally suited for medical applications, since the absorption of water in this wavelength range is quite strong ( $\sim 10^4 \text{ cm}^{-1}$ ). As human tissue contains a large amount of water, the laser penetration depth of mid-IR light is only in the order of a few or a few tens of micrometers, which allows for highly precise cutting of biological tissue. At present, pulsed lasers with a high peak power are mainly obtained by active mode locking and passive mode locking. However, 2.8  $\mu\text{m}$  mode-locked lasers are not only limited by the active and passive modulation devices, but also face the system stability problems associated with the mode-locking technology. Based on semiconductor saturable absorber mirrors and new two-dimensional material saturable absorbers such as graphene, black phosphorus and transition metal dichalcogenides, the generation of a 2.8  $\mu\text{m}$  mid-infrared fiber passive mode-locked pulsed laser has been realized. However, these saturable absorbers are faced with problems such as easy damage to devices and long-term performance degradation due to deliquescent and oxidation. In addition, the “artificial saturable absorber” material based on the nonlinear polarization rotation evolution (NPE) effect is also used to realize the generation of mode-locked pulses in the 2.8  $\mu\text{m}$  band. For NPE passive mode-locked fiber lasers, environmental factors such as external temperature and strain have a serious impact on the start and operation of mode-locking. Changes in the environment can easily change the polarization state and cause the system to lose lock. In this article, we report a 2.8  $\mu\text{m}$  mid-infrared synchronously pumped mode-locked fiber laser. This method does not require any active and passive modulation devices to be inserted into the resonator, and does not cause damages to the modulation devices. Therefore, fiber lasers based on the synchronous pump mode locking technology have high system stability and are expected to achieve an entirely monolithic mid-infrared mode-locked pulsed fiber laser.

**Methods** A 976 nm single mode pulsed laser with a high peak power is used as the pump source. When the repetition rate of the pump light is an integer multiple of the fundamental frequency of the resonator, the pump pulse generates a strong cross-phase modulation (XPM) in the fiber core to periodically modulate the signal laser phase, so that it generates sidebands and realizes mode-locking. Therefore, in this article, a 976 nm high-power single-mode pulsed fiber laser with adjustable repetition rate and pulse width is designed as the pump source, and its average output power is greater than 3 W (Fig. 1). Furthermore, a ring-cavity 2.8  $\mu\text{m}$  synchronously pumped mode-locked fiber laser is designed (Fig. 2). The optical fiber part of the experimental setup includes a 22 m long passive fiber and an 8.5 m long active fiber. These two types of fibers are spliced by using a fiber fusion splicer. There are two reasons for the fusion splicing passive optical fiber in front of an active optical fiber. On the one hand, it is to increase the working distance of 2.8  $\mu\text{m}$  signal light and pump light cross-phase modulation, and to avoid premature absorption of 976 nm pump light by  $\text{Er}^{3+}$  ions in the active fiber. On the other hand, it is to reduce the repetition rate of the laser pulse and increase the peak power of the pump light. Under this experimental structure, when the output power of the 976 nm pulsed laser meets certain requirements and the repetition rate matches the cavity length, a 2.8  $\mu\text{m}$  mode-locked pulse laser can be achieved.

**Results and Discussions** When the average power of the 976 nm pump pulse is 1.55 W, the output power of the 2.8  $\mu\text{m}$  laser is 2.5 mW and the 2.8  $\mu\text{m}$  mode-locked pulse can be observed. In the process of continuing to increase the pump power to 2.5 W, the spectrum and time envelope of the signal light do not change significantly and the maximum output power of the 2.8  $\mu\text{m}$  laser is 15 mW. When the pump power is 1.6 W, the corresponding output characteristics of the pump pulse laser (Fig. 5) and those of the 2.8  $\mu\text{m}$  pulse laser (Fig. 6) are shown in the text.



The full width at half maximum (FWHM) of pulse duration is 3.1 ns (close to the 200 MHz detector limit pulse width). The center wavelength is 2784.7 nm and the 3 dB spectral width is 0.4 nm. During the 2-hour long-term test, there is no loss of lock and the mode-locking can realize self-starting. In order to verify the principle of mode-locking, two experiments are carried out. The first is to place the 2.8  $\mu\text{m}$  intra-cavity isolator in the opposite direction. At this time, the 976 nm pump light and the 2.8  $\mu\text{m}$  signal light are transmitted in opposite directions (Fig. 6), and there is almost no XPM. In this case, mode locking is not implemented (Fig. 7), which verifies that the generation of a synchronous pump mode-locked pulse in this paper is not based on gain modulation. The second is for forward pumping. When an only 8.5 m double-clad active fiber is used in the 2.8  $\mu\text{m}$  ring cavity and other structures are the same, the 2.8  $\mu\text{m}$  mode-locked pulse cannot be obtained, which further proves the role of XPM in it.

**Conclusions** We have proposed and implemented a 2.8  $\mu\text{m}$  synchronously mode-locked pulsed fiber laser pumped by a 976 nm single-mode pulsed laser. The 2.8  $\mu\text{m}$  pulsed laser repetition rate is 6.534 MHz, the center wavelength is 2784.7 nm, the 3 dB spectral width is 0.4 nm, and the maximum output power is 15 mW. Due to the low output power, it is difficult to detect the actual pulse duration through the autocorrelator, but the oscilloscope shows 3.1 ns, which is close to the detection limit pulse width of the photodetector. Next, we will further optimize and improve the quality of the 976 nm pump light, use a fluoride fiber with a thinner core to improve the effect of cross-phase modulation, and select an active fiber with a relatively high doping concentration to increase the output power and achieve ultra-short mid-infrared mode-locked pulse. In short, based on the synchronous pump mode locking technology, there is no need to introduce any active and passive modulation devices in the resonator, and the system has a simple structure, good stability, and easy to achieve entirely monolithic fiber lasers. It provides a solution for realizing stable and reliable mode-locked pulse lasers in the mid-infrared regime.

**Key words** lasers; mid-infrared laser; synchronously pumped mode locking; cross-phase modulation